Finite size effects and scaling properties of charge fluctuations

Győző Kovács ©, 1, 2, * Pok Man Lo ©, 1, † Krzysztof Redlich ©, 1, 3, ‡ and Chihiro Sasaki © 1, 4, §

¹ Institute of Theoretical Physics, University of Wrocław,
plac Maksa Borna 9, PL-50204 Wrocław, Poland

² Institute for Particle and Nuclear Physics, HUN-REN Wigner Research Centre for Physics,
1121 Budapest, Konkoly—Thege Miklós út 29-33, Hungary

³ Polish Academy of Sciences PAN, Podwale 75, PL-50449 Wrocław, Poland

⁴ International Institute for Sustainability with Knotted Chiral Meta Matter (WPI-SKCM2),
Hiroshima University, 1-3-1 Kagamiyama, 739-8526, Higashi-Hiroshima, Hiroshima, Japan
(Dated: October 2025)

An effective model is introduced to illustrate finite volume effects beyond the usual momentum space constraints. The fluctuations of the chiral order parameter and the net baryon number, as well as their scaling properties, are investigated near a critical point and a first-order transition in finite size systems. The finite volume effects on the kurtosis are shown in detail along the approximate freeze-out line. Several implications of the finite volume in the charge fluctuations are discussed.

I. INTRODUCTION

Locating the critical endpoint (CEP) in the phase diagram of strongly interacting matter is one of the main goals of recent explorations in heavy-ion physics [1–4]. From the theoretical side, the critical behaviors at high chemical potential or baryon density can be explored using effective models formulated in the thermodynamic limit. Experimentally, the high-density region is probed with low-energy heavy-ion collisions, where the system has only a few or a few tens of fermi linear extent in the fireball. Due to the finite system size - together with other effects, such as critical slowing down, finite time – no true criticality can appear in experiments [5–10]. To observe finite-size rounding in theoretical calculations, one must either incorporate the finite-size effects within the models originally defined in the thermodynamic limit or employ frameworks that are inherently formulated in finite volumes.

However, the theoretical approaches that are naturally suited for studying the finite-size effects are typically not directly applicable at large chemical potentials, where a critical endpoint might be found. The most prominent example is lattice QCD. Although lattice calculations provide information from the first principles on the phase transition at vanishing μ , their extension to finite chemical potentials is limited due to the infamous sign problem [11, 12]. Various techniques have been invented to overcome this issue [13–18], and the system size dependence of the phase boundary at $\mu \neq 0$ has also been studied on the lattice through extrapolation from imaginary chemical potentials [19, 20]. Finite-size effects can also be implemented systematically in chiral perturbation theory (ChPT). This provides information on the size dependence

of physical quantities, e.g. meson masses, decay widths [21–23], and the quark condensate [24–28], although the results are reliable only at low temperatures and vanishing chemical potentials. Reliable modeling of finite volume systems valid at high density is mandatory to capture any signatures of a potential critical point expected in this domain.

In this work, we focus on the finite-size effects on the phase structure and charge fluctuations in an effective model that can describe the critical endpoint in the thermodynamic limit. The volume dependence of the QCD phase diagram and the hypothetical critical endpoint has already been widely studied using such approaches via momentum space constraints [29–37]. However, when these constraints are applied to a mean-field model, the divergences at the critical point cannot be removed, and the finite-size scaling is trivially absent. Here, we attempt to build a different formulation of the problem using the volume-dependent partition function directly and derive physical quantities analogously to the case of thermodynamics in a grand canonical ensemble. We employ a model featuring a critical divergence in the infinite volume limit, which is regulated in finite volumes and exhibits finite-size scaling. We study specifically the scaling behavior and finite-size effects on various charge susceptibilities and their ratios. The importance of these quantities is given by their accessibility in both theory and experiments, and their expected size (in)dependence, which together make them one of the main tools in the search for the CEP [38-42].

Our aim is solely to provide a qualitative picture of how the transition is affected when the system has a finite spatial extent from a theoretical point of view. For the emerging phenomena, we distinguish two regimes at finite sizes: First, for a finite but large volume, the noncritical quantities are almost unaffected (since dominated by the regular part), especially at low chemical potential, while the fluctuations in the vicinity of the critical point follow the expected finite-size scaling. Second, when the system size is sufficiently small (in the present work, $L \lesssim 10-20$ fm), a correction to the scaling behavior emerges,

^{*} gyozo.kovacs@uwr.edu.pl; corresponding author

 $^{^{\}dagger}$ pokman.lo@uwr.edu.pl

[‡] krzysztof.redlich@uwr.edu.pl

[§] chihiro.sasaki@uwr.edu.pl

while the thermodynamics and the phase diagram change significantly. These are genuine finite-size effects.

This work is organized as follows. In Sec. II, we introduce our framework to study finite-size effects in an effective model, based on an effective potential and the integration over a single scalar field. We also present our model setup, as well as the technical details of parametrization and scaling. Our results for the size dependence of the different physical quantities, their scaling behavior, and the phase diagram are given in Sec. III, where we also discuss the effect of the phase coexistence. Our conclusions are given in Sec. IV. An appendix is included to provide the definitions used in our framework.

II. EFFECTIVE MODEL AT FINITE SIZE

Contrary to previous approaches, we want to incorporate the finite size beyond its effect on the momentum space. We work with a realistic cubic volume $V=L^d$ with d=3 spatial dimensions, and L is the linear extent of the system. For simplicity, first we consider a case with a single scalar field $\phi(x)$. Since we aim to discuss finite temperature behavior, we start with the partition function using the Euclidean action $S(\phi) = \int_x \mathcal{L}(\phi)$ with $\int_x = \int d\tau \int d^dx$

$$\mathcal{Z} = \int \mathcal{D}\phi \ e^{-S(\phi)} \,, \tag{1}$$

and define the free energy as

$$\Phi = -T \ln \mathcal{Z} = -T \ln \int \mathcal{D}\phi \ e^{-S(\phi)} \ . \tag{2}$$

The physical quantities can be derived analogously to thermodynamics in the grand canonical ensemble as discussed in detail in App. A. Generally, the expectation value of a physical quantity \mathcal{A} is given by

$$\langle \mathcal{A} \rangle = \int \mathcal{D}\phi \ \mathcal{A} P(\phi), \qquad P(\phi) = \frac{1}{\mathcal{Z}} e^{-S(\phi)}.$$
 (3)

Carrying out the full functional integral is not possible. A naive, widely used resolution is to separate the fluctuating part of the field as $\phi(x) \to \varphi(x) + \delta \phi(x)$ with $\varphi \equiv \langle \phi \rangle$ and $\langle \delta \phi \rangle = 0$, and apply the mean-field approximation by setting $\delta \phi = 0$. In this case, there is no integration left from the functional integral, and the explicit volume dependence is lost.

Here, we keep the integration but for only a single spacetime-independent mode $\bar{\phi}$ of the field, and hence we obtain

$$\mathcal{Z} = \int_{-\infty}^{\infty} d\bar{\phi} \ e^{-\beta V \mathcal{U}_{\text{eff}}(\bar{\phi})} \,, \tag{4}$$

which can be numerically evaluated. Here, we neglect further size dependence of the action, assuming that the integration is still dominated by the minimum configuration.

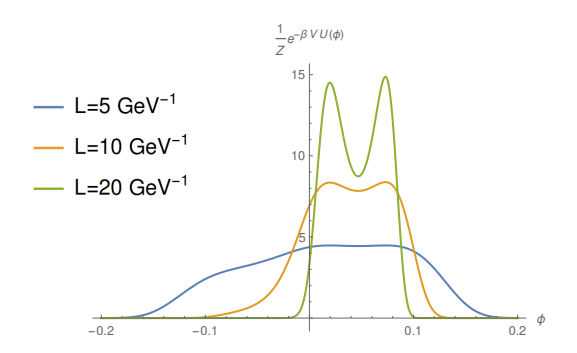


Figure 1. The $P(\phi) = e^{-S_E(\phi)}/\mathcal{Z}$ weights as a function of the field ϕ for different (rather small) system sizes close below the first-order phase boundary.

The form in Eq. (4) can be seen as a zero-dimensional field theory, and the number of degrees of freedom is reduced from infinity to one. Keeping only a single mode of the field, corresponding to vanishing momentum, is not a completely new idea to describe a thermal transition [43].

In the infinite volume limit (or at T=0), the only nonzero weight in Eq. (4) corresponds to the minimum of $\mathcal{U}_{\text{eff}}(\bar{\phi})$ as the weight $P(\bar{\phi})$ reduces to the normalized sum of Dirac deltas (two at the first order transition, one otherwise). This reproduces the usual mean-field model framework, where $\langle \phi \rangle = \bar{\phi}_0$ satisfying the field equation $(\partial \mathcal{U}_{\text{eff}}(\phi)/\partial \phi)|_{\phi=\bar{\phi}_0}=0$. However, if the system size (and the temperature) is finite, the integral over the mean-field $\bar{\phi}$ may be performed. An illustration of how the peaks in $P(\phi)$ "melt" for decreasing L is given in Fig. 1.

A. Model

To perform a numerical calculation, we can choose a specific effective potential that describes the system to be studied. Instead of providing immediately $\mathcal{U}_{\mathrm{eff}}$, we start from the level of the Lagrangian to motivate our choice. Here we use a simple model with one bosonic and one fermionic field that resembles the $N_f=1$ quark-meson model. The Lagrangian reads

$$\mathcal{L} = \frac{1}{2} \partial_{\mu} \phi \partial^{\mu} \phi - V_{\text{cl}}(\phi) + \bar{\psi} \left(i \gamma^{\mu} \partial_{\mu} - \mu \gamma_{0} - g \phi \right) \psi \quad (5)$$

with the classical potential

$$V_{\rm cl}(\phi) = \frac{1}{2}m^2\phi^2 + \frac{\lambda}{4}\phi^4 - h\phi.$$
 (6)

By integrating out the fermions, one obtains the usual functional determinant. Then the partition function is of the form of Eq. (1) with the Euclidean action

$$S_{\rm qm}(\phi) = \int_x \left(\frac{1}{2}\partial_\mu \phi \partial^\mu \phi - V_{\rm cl}(\phi)\right) - \text{Tr}\log \mathcal{S}^{-1}(\phi) \quad (7)$$

with the inverse fermion propagator S^{-1} . By keeping only the spacetime-independent mode $\bar{\phi}$, the \int_x integration becomes trivial, giving $S_{\rm qm}(\bar{\phi}) = \beta V \mathcal{U}_{\rm eff}^{\rm qm}(\bar{\phi})$. In the fermionic part, we carry out the Matsubara sum for the finite temperature calculation. Then the effective potential becomes

$$\mathcal{U}_{\text{eff}}^{\text{qm}}(\bar{\phi}, T, \mu, L) = V_{\text{cl}}(\bar{\phi}) + V_{\bar{q}q}^{v}(\bar{\phi}, L) + V_{\bar{q}q}^{m}(\bar{\phi}, T, \mu, L),$$
(8)

where the last two terms are the fermionic vacuum and matter part. These terms are generally size-dependent through the effect of the spatial extent on the momentum space and hence the momentum integral/sum $\int_{k,L}$ that gives in the infinite volume limit $\int_{k,L\to\infty}=\int\frac{d^3k}{(2\pi)^3}.$ At finite sizes, $\int_{k,L}$ is a summation over the modes determined by the spatial boundary conditions or, in a simplified scenario, a low-momentum cutoff. These cases and their proper treatment in a mean-field model are discussed in detail in [37]. The fermionic vacuum contribution

$$V_{\bar{q}q}^{v}(\phi, T, L) = -2 \int_{k, L} E(k)$$
 (9)

where $E(k)=\sqrt{k^2+m_q^2}$ with $m_q=g\bar{\phi}$ needs to be regularized. The way to handle this in the case of finite L is discussed in [37], and it turns out that we can always carry out a proper renormalization. However, due to the well-known instability for large $\bar{\phi}$ in the presence of the fermionic vacuum contribution (which dominates compared to the $\bar{\phi}^4$ term), the integration over $\bar{\phi}$ has a divergent unphysical contribution. Hence, for simplicity, here we simply neglect the vacuum fluctuations. The fermionic matter part reads

$$V_{\bar{q}q}^{m}(\phi, T, \mu, L) = -2TN_{c} \int_{k L} \left(\ln g^{+} + \ln g^{-} \right)$$
 (10)

with $g^{\pm} = (1 + e^{-\beta E^{\pm}(k)})$ and $E^{\pm}(k) = E(k) \mp \mu$. In this work, we use the quark chemical potential and symmetric quark matter hence $\mu = \mu_q = \mu_B/3$. It can be shown that for large sizes, where finite-size scaling is dominant, the momentum space constraints are already negligible. At small sizes, the effect of the volume-dependent weighting in the remnant $\bar{\phi}$ integral dominates over the modification of \mathcal{U}_{eff} due to the modified momentum integral. Furthermore, in this work, we want to focus on the yet not discussed effect of the explicit volume dependence in the partition function and the free energy. Therefore, in the following, we will completely omit the momentum space constraints for simplicity, which eliminates the size dependence of \mathcal{U}_{eff} . In the end, we remain with the size-independent effective potential

$$\mathcal{U}_{\text{eff}}(\phi, T, \mu) = V_{\text{cl}}(\phi) + V_{\bar{q}q}^{m}(\phi, T, \mu), \qquad (11)$$

which we will use subsequently. Also, from now on, we will omit the bar notation and use only ϕ .

	set A	set B	set C	set D
λ	27	28	29	32
g	4.60	4.60	4.55	4.50
$T_{\rm pc}^{\mu=0}$ [MeV]	158.4	158.0	158.5	158.5
T^{CEP} [MeV]	137.4	131.3	121.5	103.8
μ^{CEP} [MeV]	148.7	166.1	193.3	229.1

Table I. The varied parameters of the parameter sets used in the numerical calculations, the respective pseudocritical temperatures at $\mu = 0$, and the location of the CEP at $L \to \infty$.

As we focus on the qualitative investigation of the phase transition, we set the numerical value of the model parameters such that the resulting phase diagram is realistic and features a critical endpoint. To see how the location of the CEP influences the results, we include multiple parameter sets with fixed $m=-0.155~{\rm GeV}^2$ and $h=0.0018~{\rm GeV}^3$, but varying λ and g listed in Table I. At $L\to\infty$, the obtained models exhibit almost equal $T_{\rm pc}$ at $\mu=0$ and a similar phase boundary with the critical point shifted along. If not specified, the parameter set C is used.

B. Scaling behavior

We introduce the Ising thermal, external field, and leading irrelevant/marginal directions, which we denote by τ , η , and u, respectively, to avoid confusion with other quantities. The scaling ansatz for the singular part of the free energy density can be written as

$$f_s(\tau, \eta, u) = L^{-d} \mathcal{F}(\tau L^{1/\nu}, \eta L^{\beta \delta/\nu}, u L^{-\omega}). \tag{12}$$

For a general (non-negative) ω , one can keep only the leading term in L^{ω} to obtain

$$f_s(\tau, \eta) = L^{-d} \mathcal{F}(\tau L^{1/\nu}, \eta L^{\beta \delta/\nu}). \tag{13}$$

From Eq. (13), one can derive the finite-size scaling for the derivatives of the free energy, namely

$$\chi_k^{\eta} = \partial_{\eta}^k f_s = L^{k\beta\delta/\nu - d} \mathcal{F}_{\eta,k}(\tau L^{1/\nu}, \eta L^{\beta\delta/\nu}), \qquad (14)$$

and

$$\chi_k^{\tau} = \partial_{\tau}^k f_s = L^{k/\nu - d} \mathcal{F}_{\tau,k}(\tau L^{1/\nu}, \eta L^{\beta \delta/\nu}).$$
 (15)

Therefore, the finite-size scaling, for instance, for the (singular part of the) Ising-like magnetization $M=\chi_1^\eta\propto L^{-\beta/\nu}$ while for the susceptibility $\chi_2^\eta\propto L^{\gamma/\nu}$.

It is important to note that the exponents of the finitesize scaling in the form above (including the parameter dependence of \mathcal{F}) are obtained by using the hyperscaling relations. However, in the mean-field approximation in 3 spatial dimensions—which we use in this work—hyperscaling is violated, as can be seen, e.g., from $2 - \alpha \neq \nu d$ with the mean-field values. Such a scenario is known in systems above the upper critical dimension d_c [7, 9, 44]. Following Ref. [44], an effective exponent $\tilde{\nu}=(\gamma+2\beta)/d=2/3$ can be introduced, which works in the scaling formulas also in the case below the upper critical dimensions but with mean-field approximation. We emphasize that the introduction of $\tilde{\nu}$ serves merely to shorten our notation and keep the well-known simple expressions.

The above discussion of the scaling behavior relies on the singular part of the free energy and the derived quantities. However, our free energy in Eq. (2) also contains a regular part $\Phi_{\rm reg}$ that generally scales as L^d and hence analogously to Eq. (12) $f_{\rm reg}(\tau,\eta) \propto L^0$, which is also inherited by the derivatives. Therefore, this contribution dominates the scaling of the free energy itself and of its first derivatives, since, e.g., $\beta\delta/\tilde{\nu}-d<0$. To study the scaling in these cases, the regular part shall be subtracted.

To use the finite-size scaling ansatz, the Ising directions have to be identified in the parameter space of our model, spanned by T, μ , and h. Usually, the external field h (corresponding to the current quark mass) is fixed, and hence, the irrelevant direction is absent on the remaining surface. Then the Ising temperature and field-like directions can be obtained in the vicinity of the CEP via a linear map in T and μ [45]. However, from the scaling, it turns out that the η direction has a nonzero overlap with each h, T, and μ . Each of them holds a field-like scaling, and the generalized susceptibilities, χ_k , χ_k^B , and χ_k^T (defined by the k^{th} derivative in the h, μ , and T directions, respectively) have the same volume dependence. Consequently, the order parameter, the chiral susceptibility, the baryon number, entropy, and energy density (and their fluctuations) show the scaling dominated by the η -derivatives. It is also expected that the temperature-like scaling will be observable only in directions along the phase boundary (or phase boundary surface if h is considered) in a narrow window for a linear sigma model [46]. Similarly, the trivial scaling is observed only when moving very closely along the marginal direction u. Note that the critical exponents in the T and μ direction do not depend on the treatment of h and hence on the actual choice of τ and η (being a function of h or not). However, the form of the scaling function is different in different directions, even if having the same η -like and τ -like scaling.

III. FINITE SIZE DEPENDENCE

Using the simple model outlined above, we discuss the size dependence of the phase diagram, different physical quantities, and their fluctuations. We start with the chiral condensate and susceptibilities and discuss the finite-size scaling on their example. One can also look at the scaling properties of the baryon number fluctuations. However, as discussed above, these show the same qualitative behavior.

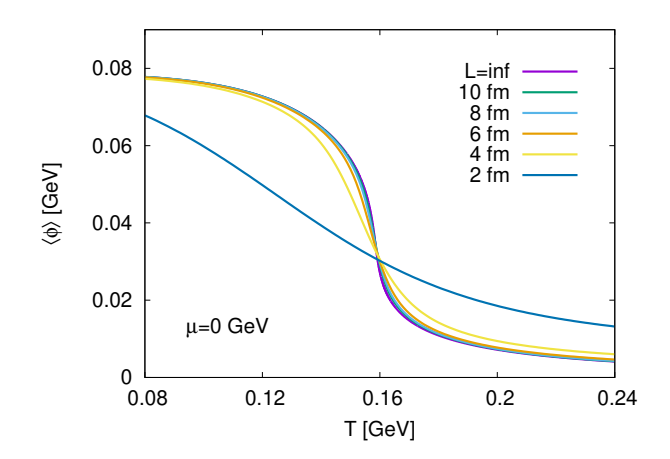


Figure 2. The chiral condensate $\langle \phi \rangle$ at $\mu = 0$ for different system sizes and in the thermodynamic limit.

A. Chiral condensate and susceptibility

First, we discuss generally the effect of the finite size on the chiral condensate, which immediately highlights the limitations and the advantages of our approach. At nonvanishing temperatures, it is generally clear from our formalism that the weights in Eq. (A1) tend to become equal for any $\phi \in (-\infty, \infty)$ for $L \to 0$ since the exponential tends to unity, independently of the field. Therefore, in the chirally broken region, $\langle \phi \rangle$ decreases for a small, decreasing L. As shown in Fig. 2 for $\mu = 0$, this also gives rise to a decrease of the pseudocritical temperature as the crossover between the phases shifts for $L \leq 10$ fm. However, at $T \to 0$ there are no finite-size effects due to the statistical weighting, since the full four-volume βV tends to infinity. Therefore, the vacuum value of $\langle \phi \rangle$ is constant in L. This caveat of the model leads to the main difference compared to lattice results, where an exponential rise of the chiral condensate is found for very small sizes [19, 20]. The normalized condensates already show the same dependence at finite T and L. This again suggests that the main difference comes from $\langle \phi \rangle$ in the vacuum being constant and anticipates that the phase boundary behaves similarly when the size decreases. However, the size dependence of $\langle \phi \rangle$ also determines that of the susceptibility, for which we see a decreasing maximum due to the softening of the transition, unlike on the lattice.

Interestingly, the ChPT calculations provide a decreasing trend in the quark condensate [24, 26], even in the regime of the ϵ expansion [25, 27], which becomes relevant for $L \lesssim 2$ for the physical pion mass. One can see an exponential dependence in ChPT—similar to that in the lattice calculations, but with opposite sign—with also an interesting interplay with a finite magnetic field [28].

¹ In the chirally restored region close to $T_{\rm pc}$, due to the emerging nonzero weight of the $\phi > \phi_0 \sim 0$ contribution, $\langle \phi \rangle$ is increasing unless the size is very close to zero.

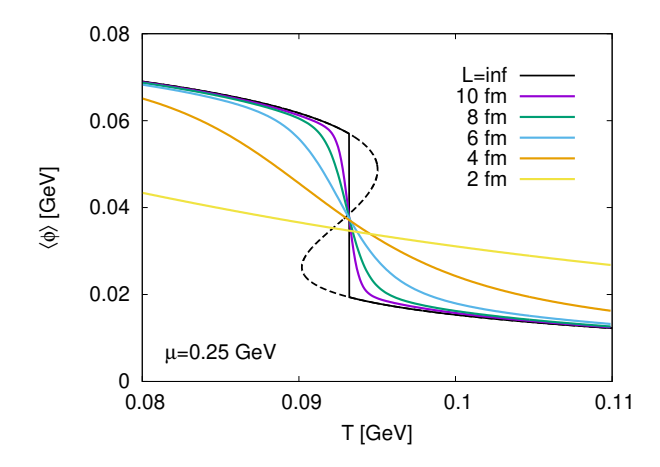


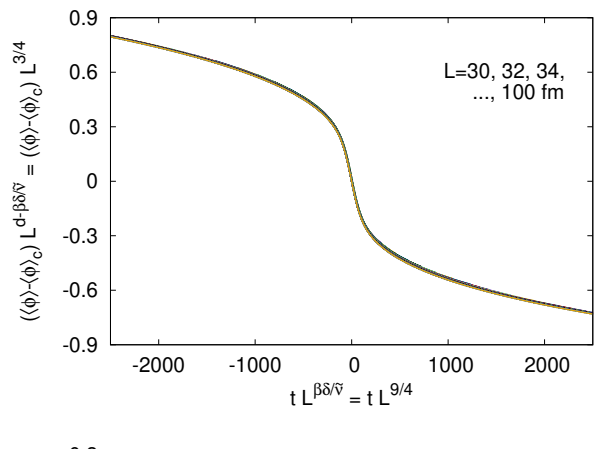
Figure 3. The chiral condensate $\langle \phi \rangle$ at a first-order transition for different system sizes and in the thermodynamic limit. The dashed curve shows the $L \to \infty$ meta- and unstable solutions.

Functional methods with momentum space constraints also predict the decrease of the chiral condensate for very small sizes [32].

We emphasize that these effects in the crossover region are not due to the scaling, but really are finite-size effects. We also note that the inclusion of momentum space constraints (when applied also to the vacuum fluctuations) could give rise to a size-dependent $\langle \phi \rangle_{T=0}$ as well, since they modify the potential \mathcal{U}_{eff} itself. However, the magnitude and even the direction of this effect depend on the chosen type of constraint, on the boundary condition, and in certain L intervals, even on the treatment of the vacuum contribution [36, 47].

At high chemical potentials, the phase transition for $L \to \infty$ is of first order in our model. However, at finite sizes there is always only a single solution, and the transition is smooth for any finite L as shown in Fig. 3.² This is in contrast with the case when the finite-size effects are implemented in a mean-field model only via momentum space constraints, because it is still based on the minimization of a modified $U_{\rm eff}$, featuring unstable and metastable solutions and a sharp transition. A similar smoothing was also recently seen in Ref. [48] within a different framework.

Since the phase transition becomes smooth in our framework, there is also finite-size rounding of the susceptibility at the critical point, and we can investigate the scaling behavior. As discussed before, one shall take care of the regular part of the free energy. It is sufficient to ap-



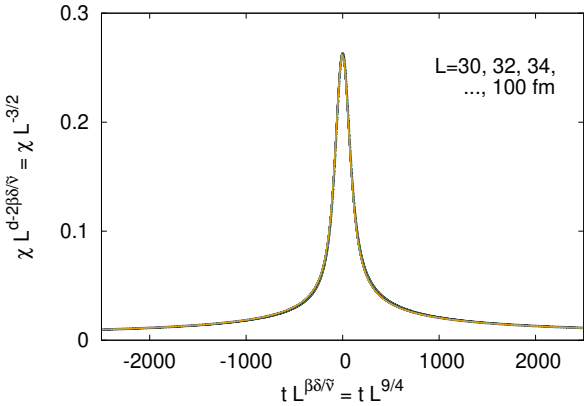


Figure 4. The $L=30,\,32,\,34,\ldots,\,100$ fm results collapsing to a single curve for the singular part of the chiral condensate (top) and the chiral susceptibility (bottom) as a function of the scaled subtracted temperature.

proximate $f_{\rm reg}$ with a linear ansatz,³ which brings only a constant $\langle \phi \rangle_c \equiv \langle \phi \rangle|_{T^{\rm CEP},\mu^{\rm CEP}}$ subtraction from $\langle \phi \rangle$, while χ —which is anyway dominated by the singular part—is unchanged. The obtained finite-size scaling is presented in Fig. 4 through the $L \to \infty$ critical point as a function of the reduced temperature $t = (T - T_c)/T_c$ scaled with the appropriate power of L. As discussed in Sec. II B, since both h and T have overlap with the η direction, we need to use the external field-like scaling exponents. The results collapse to a single curve, which shows scaling is for $L \gtrsim 100~{\rm GeV}^{-1} \approx 20~{\rm fm}$. For these sizes, the shift in the transition temperature is negligible, while for $L \lesssim 20~{\rm fm}$, the finite-size effects emerge.

It is interesting to study the susceptibility also in the vicinity of the $L \to \infty$ first-order transition. It turns out that the coexistence—in our case, the presence of two

 $^{^2}$ Due to the discussed unchanged behavior at T=0, the phase transition at vanishing temperature remains sharp and effectively serves as an endpoint.

³ One may try to fit $f_{\rm reg} + f_s$ in the infinite volume case. In the T, μ, h parameter range of interest, the linear ansatz works properly. Higher order terms give only negligible corrections in Φ , $\langle \phi \rangle$, and χ , while terms beyond quadratic order cannot even be fitted reliably.

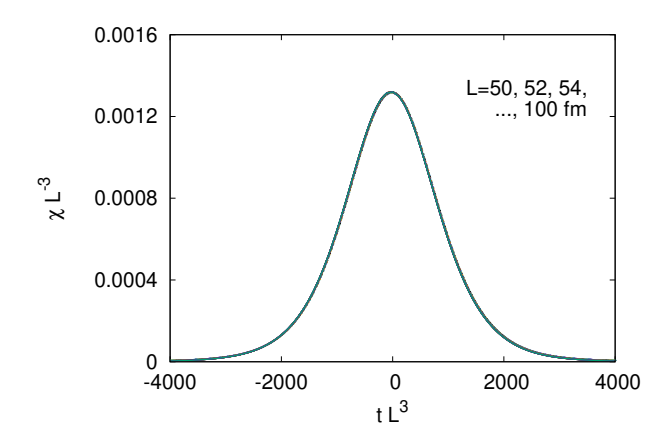


Figure 5. The scaled chiral susceptibility as a function of the scaled temperature in the neighborhood of the first-order transition.

equal minima of the potential—gives rise to nontrivial volume dependence. While the chiral condensate remains $\langle \phi \rangle \propto L^0$, the susceptibility obtains a $\chi \propto L^d$ (generally $\chi_k \propto L^{k\,d}$) scaling in the vicinity of T_c . This scaling behavior is shown in Fig. 5. The phenomenon can be easily understood by using a double Gaussian approximation for the probability distribution [7], which we also review below in Sec. IIIB. Due to the $\chi_k \propto L^{k\,d}$ size dependence driven by the coexistence in the first-order case, the peak of the chiral susceptibilities monotonously increases for increasing μ along the phase boundary. Thus, no apparent critical endpoint can be identified purely as a maximum of χ as done in functional methods with momentum space constraints [33, 34, 49]. To locate the $L \to \infty$ critical endpoint, one needs other tools such as the binder cumulant, which we discuss in detail in Sec. III E.

We note that involving also the momentum space constraints in $\mathcal{U}_{\rm eff}$ in Eq. (11) does not modify the scaling behavior (which we checked also numerically), since the effect of the cutoff or discretization becomes relevant when the finite-size effects emerge. This is expected only for sizes below $L \approx 10-20$ fm.

In the infinite volume mean-field calculation, it is usual to determine also the curvature mass of the meson field. The critical mode at the chiral CEP (in the absence of further condensates [50]) corresponds to the scalar singlet σ (here ϕ itself), for which the mass squared is equal to the inverse of the chiral susceptibility. It is usual to use this relation to define the meson mass at finite system sizes by $m_\phi^2 = \chi_2^{-1}$ (or vice versa), which shall be nonzero when χ_2 does not diverge. We emphasize that this is not equivalent to naively extending the infinite size definition $m_{\phi,L\to\infty}^2 = \partial^2 \mathcal{U}_{\rm eff}/\partial \phi^2$ and calculating the expectation value of the curvature of the effective potential. The mass, defined with the susceptibility, does not have a minimum around the $L\to\infty$ critical point for finite L due to the coexistence. Since the expectation value of the curvature of $\mathcal{U}_{\rm eff}$ has no effect from the coexistence, it exhibits a

minimum. However, this quantity does not correspond to the two-point function, from which the curvature mass might be obtained in the vanishing momentum limit.

B. Effects of the coexistence

In the first-order transition at finite sizes, the susceptibility exhibits a $\chi \propto L^d$ divergence for $L \to \infty$. This divergence stems from the coexistence, which is a known phenomenon [8] that we discuss in our approach. This also provides an opportunity to define an η direction everywhere on the phase boundary.

To understand the role of the coexistence in the finite size scaling, following [6, 8], one can start with a double Gaussian approximation, assuming two minima at $\phi = \sigma_a$ and σ_b with "susceptibility" (the curvature $\chi_i = \partial^2 \mathcal{U}(\phi)/\partial \phi^2|_{\phi=\sigma_i}$ for i=a,b) χ_a and χ_b , respectively, at the first order transition (i.e., at $\eta=0$). This is a good approximation of the full probability distribution obtained from the potential in the vicinity of the minima, which are more dominant for large sizes. By expanding \mathcal{U}_{eff} at $\eta=0$ in ϕ around the minima, one can write the probability density in the form ⁴

$$P_{DG}(\phi) = \frac{A}{(2\pi T)^{1/2}} \times \left[e^{(\eta \sigma_a + \frac{1}{2}\eta^2 \chi_a) \frac{L^d}{T}} e^{-\frac{(\phi - \sigma_a - \eta \chi_a)^2}{2\chi_a} \frac{L^d}{T}} \right] + e^{(\eta \sigma_b + \frac{1}{2}\eta^2 \chi_b) \frac{L^d}{T}} e^{-\frac{(\phi - \sigma_b - \eta \chi_b)^2}{2\chi_b} \frac{L^d}{T}} ,$$
(16)

with an appropriate normalization

$$A = L^{d/2} \left[\chi_a^{1/2} e^{(\eta \sigma_a + \frac{1}{2}\eta^2 \chi_a) L^d / T} + \chi_b^{1/2} e^{(\eta \sigma_b + \frac{1}{2}\eta^2 \chi_b) L^d / T} \right]^{-1}$$
(17)

to satisfy $\int_{-\infty}^{\infty} d\phi \, P_{DG} = 1$. T is the (not reduced) Ising temperature. Then, one can calculate $\langle \phi \rangle$ and $\langle \phi^2 \rangle$ (and hence χ) analytically via the Gaussian integrals over ϕ . This leads to

$$\langle \phi \rangle_{DG} = \lambda_a U_a + \lambda_b U_b ,$$

$$\chi_{DG} = \chi_a U_a + \chi_b U_b + \frac{L^d}{T} (\lambda_b - \lambda_a)^2 U_a U_b ,$$
(18)

where $\lambda_i = \sigma_i + \eta \chi_i$, $U_i = W_i/(W_i + W_j)$ and $W_i = \sqrt{\chi_i} \exp\{(\eta \sigma_i + \eta^2 \chi_i/2) L^d/T\}$ with $j \neq i$. From the first line of Eq. (18) it can be seen that $\langle \phi \rangle_{DG}$ is a weighted sum of the contribution from the two minima, depending on not only the σ_i , but also χ_i . At the transition, i.e., $\eta = 0$ the weights are exactly 1/2 if $\chi_a = \chi_b$.

⁴ The simplified form, e.g., shown in Ref. [8], can be written in the symmetric $\chi_1 = \chi_2$ case.

Contrary to $\langle \phi \rangle_{DG}$, the susceptibility χ_{DG} is not only a weighted sum, but also contains a $\propto L^d$ contribution that characterizes fluctuations between the two minima. Along the phase boundary $(\eta = 0$, hence $\lambda_i \to \sigma_i)$ this contribution depends on the difference $(\sigma_b - \sigma_a)^2$. Therefore, when approaching the critical endpoint with increasing T, the effect of the coexistence clearly becomes absent at the CEP.

To use the double Gaussian formula in our approach, we can map the T, μ , and h variables to T and η . Instead of the linear ansatz, valid only in the vicinity of the CEP, we try to find a geometric construction that can be used at any point of the phase boundary surface and fits the construction of the double Gaussian form in Eq. (16). For this, one may consider the following: Let us have the effective potential in the form

$$\mathcal{U}(\phi; T, \mu, h) = u(\phi; T, \mu) - h\phi. \tag{19}$$

First, we expect a phase transition at h = 0 (for any T and μ) between the minima at $\phi = \pm \phi$ being global minimum for h > 0 and h < 0, respectively. However, here we aim to study a phase transition at a nontrivial T, μ, h surface with finite T_c, μ_c, h_c (parameters with subscript c mark here a given point of the phase boundary surface). Assuming that the minima of the potential are ϕ_a , ϕ_b at the transition with a maximum at ϕ in between (for a crossover, the transition might be defined such that $\phi = \phi$ is the solution at T_c, μ_c, h_c). Therefore $\mathcal{U}'(\phi, T_c, \mu_c, h_c) =$ $u'(\tilde{\phi}, T_c, \mu_c) - h_c = 0$. Of course, $\tilde{\phi} = \tilde{\phi}(T, \mu, h)$, i.e., the phase boundary depends nontrivially on each parameter. To find the coupling of the linear field dependence, one can expand in $\varphi = \phi - \phi$ (this mapping is again parameter dependent due to the dependence of ϕ) around zero or, equivalently, in ϕ around ϕ

$$\mathcal{U}(\phi; T, \mu, h) = \mathcal{U}(\tilde{\phi}; T, \mu, h) + \mathcal{U}'(\tilde{\phi}; T, \mu, h)(\phi - \tilde{\phi})$$

$$+ \frac{1}{2}\mathcal{U}''(\tilde{\phi}; T, \mu, h)(\phi - \tilde{\phi})^{2} + \dots$$

$$= \tilde{\mathcal{U}}(\phi - \tilde{\phi}, \tilde{\phi}; T, \mu, h) - \eta(\tilde{\phi}; T, \mu, h)(\phi - \tilde{\phi})$$

$$= \tilde{\mathcal{U}}(\varphi; T, \mu, h) - \eta(T, \mu, h)\varphi,$$
(20)

where we implicitly defined $\tilde{\mathcal{U}}$ and

$$\eta(T,\mu,h) = h - u'(\tilde{\phi},T,\mu), \qquad (21)$$

and also simplified the dependence through $\tilde{\phi} = \tilde{\phi}(T, \mu, h)$ to ease the notation. The form in the last line of Eq. (20) with the field φ and the external field η has the same properties near the transition at T_c, μ_c, h_c as the original form of \mathcal{U} in Eq. (19) with the field ϕ and the external field h near the transition at h = 0. Namely, the hase transition happens at $\eta = \eta(T_c, \mu_c, h_c) = 0$, while $\varphi = 0$ is the unstable solution at the first-order transition between ϕ_a to ϕ_b (or the solution for a crossover transition). Moreover, the higher-order terms in φ vanish at the critical point (along the critical line) since there $\partial^n \mathcal{U}/\partial \phi^n|_{T_c,\mu_c,h_c,\tilde{\phi}} = 0$

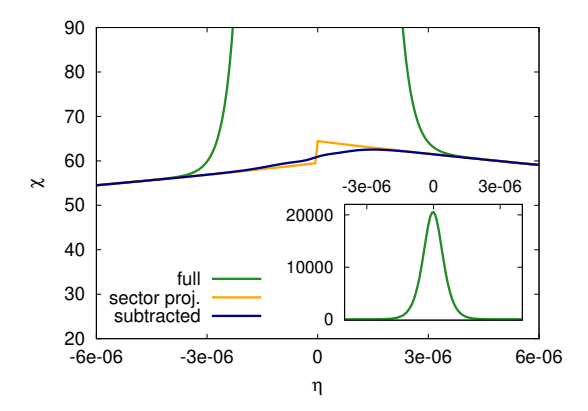


Figure 6. The chiral susceptibility as a function of $\eta(T,\mu,h)$ at $\mu=220$ MeV. The green line is the full result calculated at $L=250~{\rm GeV^{-1}}\approx 50$ fm (also shown in the inset to see its full height), while the blue curve is the remnant after subtracting the divergent part as discussed in the text. The orange line is the sector projected result for the two minima.

for $n \in \mathbb{Z}^+$. Of course, this mapping is not perfect, since the potential is not symmetric in φ around $\varphi = 0$. For instance, $\chi_a \neq \chi_b$ remains unchanged in the two minima. However, effects comming from assymetry beyond the properties of te minima are suppressed for sufficiently large L.

Now we need to relate the change of $\eta(T, \mu, h)$ defined in Eq. (21) to the change of its arguments. The simplest approximation is to compare $\partial_x \eta$ for x = T, μ , and h, which is equivalent to expanding in T and μ up to linear order. This gives $d\eta = -dh$, $d\eta \approx 0.078 (\text{GeV}^2) dT$, and $d\eta \approx 0.039 \, (\text{GeV}^2) \, d\mu$ at the first-order transition at $T_c = 0.10942 \text{ GeV}, \ \mu_c = 0.220 \text{ GeV}, \ h_c = 0.0018 \text{ GeV}^3.5$ Instead of discussing $\chi(T)$ with the relation between T and η —in which case one shall take care of the change of T due to the change of the temperature T as well—it is more convenient and straightforward to use $\chi(\eta)$ directly, using the above evaluated $\eta(T, \mu, h)$ dependence. We note that T still has to be determined, which we simply obtain from fitting χ_{DG} to the calculated $\chi_{\rm calc}$ as T ≈ 0.11 GeV.⁶ As shown in Fig. 6, with careful parametrization of the double Gaussian formula, the calculated susceptibility can be not only fitted, but the coexistence peak can even be

⁵ From such an approximation evaluated at the CEP it is clear again that η has a nonzero overlap with each $x=T, \mu$, and h. Note that the magnitude of the $d\eta/dx$ ratios shall not be directly compared due to the different dimensionality and absolute magnitude of the parameters themselves.

⁶ The subtracted temperature τ , might be approximated analogously as in a Landau-type potential. Then, τ is related to the second field derivative of the potential $u''(\tilde{\phi}, T, \mu)$, up to an overall scale.

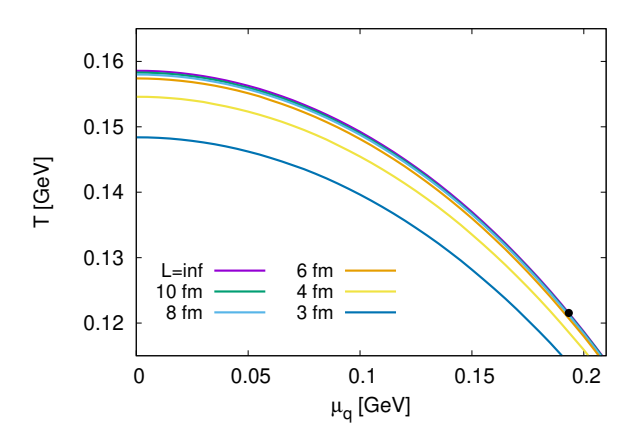


Figure 7. The chiral phase boundary obtained by the maximum of the chiral susceptibility for different system sizes. The black dot marks the $L \to \infty$ CEP.

removed⁷ by defining

$$\chi_{\text{subt}} = \chi_{\text{calc}} - \frac{L^d}{T} (\lambda_b - \lambda_a)^2 U_a U_b.$$
 (22)

After removing the three orders of magnitude higher peak, only a small fluctuation remains close to the transition due to the assumptions we have made. Namely, the value of σ_i and χ_i in the minima are not constant when moving away from the phase transition. The potential is not symmetric in φ around $\tilde{\phi}$. The change of T, μ , and h changes η and also T nonlinearly. And finally, unless the volume is extremely large, there is a correction to the double Gaussian approximation itself. To sample the contribution from the two minima separately, one can use sector projection by integrating separately for $\phi \leq \tilde{\phi}$ and $\phi > \tilde{\phi}$. For sufficiently large sizes, this can reproduce the contribution from the two (even local) minima separately, between which $\chi_{\rm subt}$ interpolates.

Finally, we note that a real physical system is not expected to stay long in a state where the two phases coexist in a first-order transition. Hence, the effect of the coexistence might be less dominant for the experimental results even at finite volumes.

C. Phase diagram

In relation to the size dependence of $\langle \phi \rangle$ in Fig. 2, we already mentioned that the phase diagram modifies when the finite-size effects become important. At finite L, just as in the case of the $L \to \infty$ crossover, we determine the phase transition by the maximum of the chiral susceptibility. The emerging phase boundaries—shown in

Fig. 7—match surprisingly well⁸ with the size dependence of the lattice results [19, 20], obtained by extrapolation from imaginary chemical potentials. For low μ the transition temperature starts to deviate from the $L \to \infty$ value around L = 5 - 6 fm with an approximately 6.5 % decrease at L=3 fm. For very large μ , the gap between the phase boundaries at different sizes shrinks, but remains present, contrary to the lattice results. While our simple model has obvious limitations for high μ —for instance, the absence of the baryons or the meson fluctuations—the extrapolation used in the lattice calculations also works better for lower chemical potentials. We note that the system size, where the phase transition deviates from the infinite size value, is determined in our approach by when the weights in Eq. (4) become important around (and below) $\phi \approx 0$ at the temperatures $T \sim T_{\rm pc}$. Hence, it is sensitive to the external field h, which raises the $\phi < 0$ minima and deepens the $\phi > 0$ minima of the potential.

D. Thermodynamics

For completeness, we also investigate the finite-size effects on the thermodynamics. As discussed earlier, due to the limitations of our approach, there is no effect at T=0, which draws two consequences. First, we cannot study the size dependence of the equation of state at vanishing temperature as a function of μ . Note that our quarkmeson-like model would anyway be missing important ingredients in this regime (e.g., baryons), while the physical systems in this direction (e.g., compact stars) are not expected to be small enough to be strongly affected. Second, at T=0, the pressure and all thermodynamic quantities are constant in L. However, at small but nonzero T, the averaging over ϕ has a nonzero contribution from $\phi \neq \phi_0$ with $p < p(\phi_0)$ and hence the pressure decreases. This leads to a nonphysical decrease of p for small increasing temperature. However, this effect is limited to very small temperatures far from the phase transition unless the system size becomes extremely small. Similar to the phase boundary, the thermodynamics does not change reasonably until $L \approx 10$ fm is reached, as shown in Fig. 8 for $\mu = 0$. When the finite-size effects become important, the pressure (and similarly the entropy density) decreases for the reasons mentioned above. The different contributions in the energy density ϵ compensate each other in such a way that it remains relatively constant with only a slight decrease for $T > T_{\rm pc}$ and a slight increase for $T < T_{\rm pc}$. Consequently, the $p(\epsilon)$ curve moves downwards and also becomes softer for decreasing L, which is also shown in Fig. 8. A similar behavior can be found in the vicinity of the CEP and at the first-order transition. The latter case is interesting as the pressure interpolates between the

⁷ For a proper subtraction, the parameters have to be determined very precisely.

⁸ Although the resuts are similar also quantiatively, since our framework is suitable for more of a qualitative investigation, the similarity shall also be treated at a qualitative level.

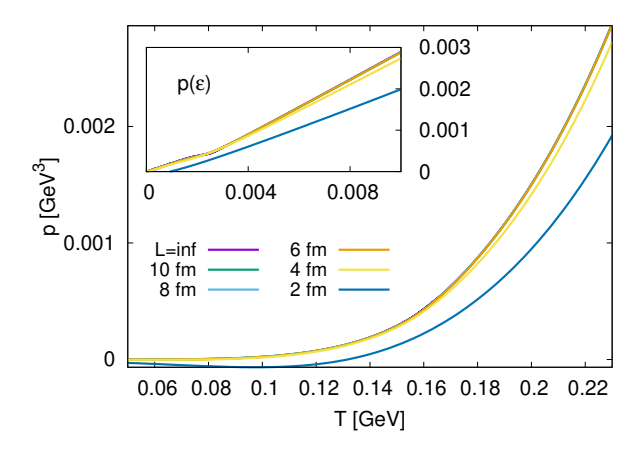


Figure 8. The pressure with the T=0 contribution subtracted as a function of temperature and of the energy density (inset) for different system sizes.

branches of the two stable mean-field solutions. However, this interpolation is always below the $L \to \infty$ pressure, just as in the $\mu = 0$ case.

E. Fluctuations along the phase boundary

As we discussed in Sec. III A, the extrema of the different order susceptibilities monotonically increase along the phase boundary, due to the scaling in the secondand first-order phase transition. Accordingly, to study the vicinity of the CEP, one needs a ratio of the susceptibilities (or cumulants) that is size independent. To this end, one can define the Binder cumulant (of the chiral susceptibility)

$$\kappa_B = \frac{\chi_4}{\beta L^d \chi_2^2} \,, \tag{23}$$

which scales as L^0 at both the second-order and firstorder transition [5]. The presence of the $\beta = 1/T$ factor in the present approach is related to the role of the four-volume βV in our framework. Although the definition would be sufficient for scaling without this factor, it is important for the universal limiting values for large and small τ . As shown in Fig. 9, κ_B is indeed independent of the system size and extrapolates between the Gaussian result $\kappa_B \to 0$ of the crossover and $\kappa_B \to -2$ obtained from a two-peaked probability approximation of the first order case. If the τ parameter—which we can approximate in such close vicinity of the CEP by $\tau = \text{sgn}(T - T^{\text{CEP}})\sqrt{(T - T^{\text{CEP}})^2 + (\mu - \mu^{\text{CEP}})^2}$, when h is kept fixed—is not rescaled with the finite size, the κ_B curves calculated at different system sizes are expected to cross each other at the critical point, which can also be used to identify the CEP when the thermodynamic limit cannot be reached [7, 51]. In our case, this method recovers the $L \to \infty$ CEP as expected, as shown in the inset of Fig. 9.

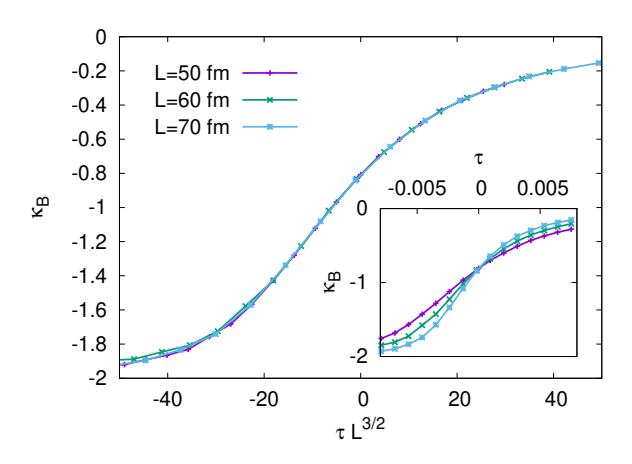


Figure 9. The binder cumulant along the phase boundary as a function of $\tau L^{1/\tilde{\nu}}$ for different sizes. The inset shows the same curves but as a function of the unscaled τ .

From the above discussion, it is clear that the usually used susceptibility ratio χ_4/χ_2 – and equivalently χ_4^B/χ_2^B , used also in Refs. [37] and [52] – is appropriate only outside of the scaling region, but should be volume dependent in the vicinity of the CEP. This is in line with the finite-size scaling that predicts $\chi_4/\chi_2 \propto L^{2\beta\delta/\tilde{\nu}} = L^{9/2}$ near the critical point, in contrast to $\chi_4/\chi_2 \propto L^0$ far from it, for instance, at the freeze-out line.

F. Fluctuations along the freeze-out line

For the experimental relevance of the finite size effects, we investigate the physical quantities also along the freezeout line, where nonmonotonicity of the cumulant ratios is expected in the presence of a critical endpoint [4, 38–40]. Since this line is outside of the scaling region, one expects $\kappa_k \propto L^d$ for the $k^{\rm th}$ cumulant and hence $\chi_k \propto L^0$ for the corresponding susceptibility. Therefore, one may use the cumulant (and therefore equivalently susceptibility) ratios $\kappa_k/\kappa_l \sim \chi_k/\chi_l$ with $l, k \neq l \in \mathbb{Z}^+$, which behave as $\propto L^0$ when the finite-size scaling dominates. Moreover, instead of using the temperature or baryon chemical potential, these parameters can be related to the \sqrt{s} center of mass energy according to the parametrization in Ref. [53]. The freeze-out line itself can be directly obtained from $T(\sqrt{s})$ and $\mu(\sqrt{s})$ [53] as

$$T_{\text{fo}}(\mu) = T_{\text{fo}}^0 / (1 + \exp\{a - b \ln(\mu_0/\mu - 1)\}),$$
 (24)

or we can use a simple quartic form

$$T_{\text{fo}}(\mu) = T_{\text{fo}}^0 - \alpha \mu^2 - \beta \mu^4,$$
 (25)

with $\alpha, \beta > 0$ as in Ref. [54]. In the former case, $T_{\rm fo}$ starts to decrease very slowly with the increasing chemical potential. In this case, if $T_{\rm pc}|_{\mu=0} = T_{\rm fo}^0$ is set, the freeze-out line would overgrow and then cross the transition line, which is rather unexpected in the physical case. Instead

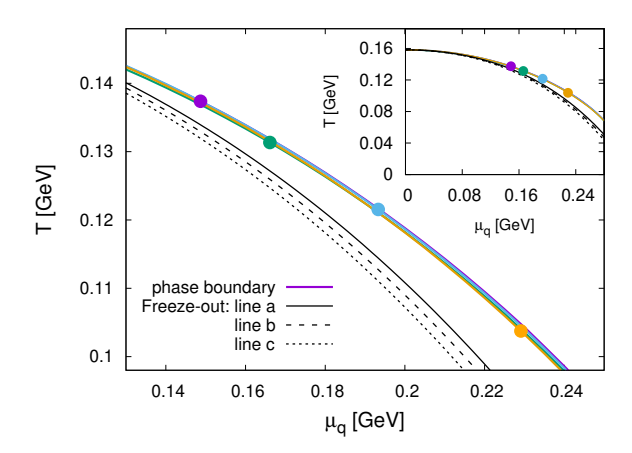


Figure 10. The phase boundaries with the $L \to \infty$ CEP for the parameterizations in Tab. I and the three freeze-out line parametrization we use.

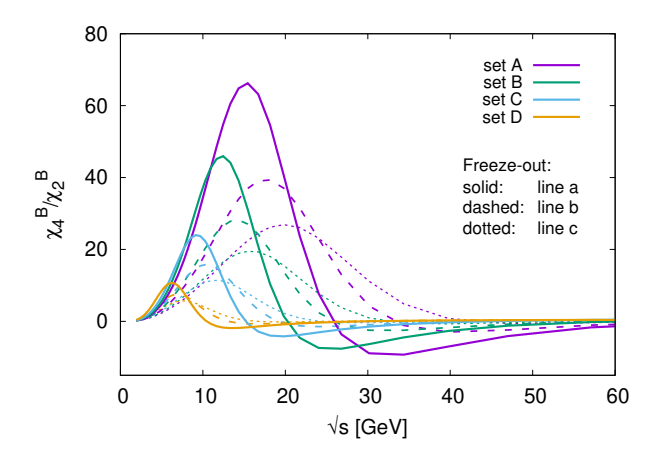


Figure 11. The R_{42} baryon number cumulant ratio along the freeze out lines shown on Fig. 10 calculated with the different parameterizations at infinite size.

of manipulating the parameters of Eq. (24), which would also alter the $\sqrt{s}(\mu)$ dependence, we use the quartic form in Eq. (25). The freeze-out temperature at $\mu = 0$ is set to the pseudocritical temperature. Since there is an uncertainty in both the exact location of the freeze-out line and the phase boundary at large chemical potential, we try multiple parameterizations. Fixing $\beta = 0.06$, we use $\alpha = 0.110$, 0.115, and 0.120 labelled as line a, b, and c, respectively. To test the effect of CEP at different locations, we also use multiple parameter sets (see Tab. I). The obtained phase transition lines are (almost) on top of each other, while the CEP is shifted as shown in Fig. 10, where the freeze-out lines are also depicted. Since usually the baryon fluctuations are discussed, we use them instead of chiral susceptibilities here, even though they exhibit the same behavior qualitatively. We show the "kurtosis" $R_{42} = \chi_4^B/\chi_2^B$ calculated along the different freeze-out with the different parameterizations on Fig. 11. As the relative separation between the freeze-out curve and the

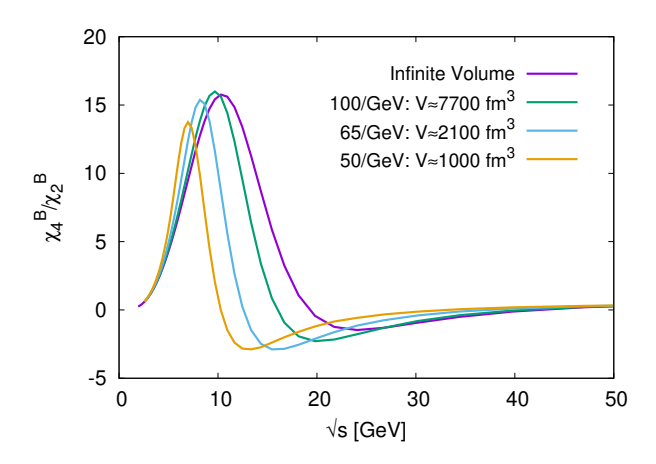


Figure 12. The χ_4^B/χ_2^B susceptibility ratio at different sizes along the freeze-out line b using the parameter set C.

phase boundary becomes wider, the amplitude of the signal decreases significantly. This behavior highlights the importance of the distance of the CEP from the freezeout. To discuss the finite size dependence, we choose line b and the parametrization with set C. The obtained behavior is shown in Fig. 12. The infinite volume dip-peak structure remains and becomes only slighly smaller even for $L = 50 \,\mathrm{GeV}^{-1} \approx 10 \,\mathrm{fm}$ (which is the smallest expected size), but it is shifted to lower \sqrt{s} for sufficiently small L. For linear sizes $L \gtrsim 200~{\rm GeV}^{-1} \approx 40~{\rm fm}$ there is no finite size effect, and practically, the $L \to \infty$ behavior is seen. It is interesting to contrast the finite sizes to which the fluctuations and the phase boundary are sensitive. From Fig. 7 it is clear that above $L \approx 10$ fm there is only a very mild change in the phase transition, while the fluctuations are already sensitive below $L \approx 40$ fm. However, from Fig. 11 it is also clear that already a small change in the relative location of the freeze-out line and the phase boundary can strongly affect what we see on the freeze-out line.

Although the shift in the dip-peak structure due to the finite-size effects is moderate, we emphasize that the observation of such a structure in Fig. 12 might not be sufficient to identify a critical point. Especially when the coexistence gives such a dominant contribution as in our approach. Recall that at finite system sizes, the extremum values of the susceptibilities and hence of R_{42} show a monotonic increase/decrease for increasing μ . Hence, from the point of view of a finite-size system, the origin of the dip-peak structure along the freeze-out line is simply the separation of the phase boundary and the freeze-out. Therefore, it is not trivial to tell if the vicinity of an $L \to \infty$ critical point is reached at finite L unless further information is known.

Finally, we note that there is an interesting region between the phase boundary discussed in Sec. III E, and the freeze-out line discussed here. Since in a given L range, the extent of the finite-size scaling region for χ_4 turns out to be larger than that for χ_2 , there is a part of

the phase diagram, where the former still shows critical L-scaling, while the latter is already $\propto L^0$. This gives rise to a peculiar scaling behavior that cannot be described by χ_4/χ_2 or κ_B . However, not only the size and location, but even the existence of this interesting region is clearly model-dependent.

IV. CONCLUSION

We studied the finite-size effects in a schematic quarkmeson type model based on the size dependence of the partition function and the free energy. These quantities are defined using the size-dependent integration such that the non-trivial finite-volume effects remain in the functional integral. In this approach, we are able to recover the correct scaling behavior at the critical point, while it also highlights the even stronger volume dependence of the fluctuations at the first-order transition caused by the phase coexistence. From the critical scaling for the different susceptibilities, χ_k , χ_k^B , χ_k^T , it follows that each T, μ , and h has an overlap with the Ising external field-like scaling direction. This can also be seen within more complex models (e.g., advanced versions of the quark-meson model [55]) by studying the critical scaling at $L \to \infty$.

The phase boundary, determined by the peak of the chiral susceptibility, moves to a lower temperature as the system size decreases in line with the lattice results [19]. We also see such a trend for large baryon-chemical potentials. Due to the monotonic increase of χ with increasing chemical potential along the phase boundary because of the coexistence, no apparent critical endpoint can be identified by the maximum of the susceptibilities. This behavior is expected for the properly defined susceptibility [8], but in contrast to the models incorporating finite-size effects only via momentum space constraints [33, 34]. The criticality in $L \to \infty$ can be identified by the Binder cumulant, which we discussed along the phase boundary. Along the freeze-out line, which lies completely outside the scaling region in our model, we studied the kurtosis ratio $R_{42} = \chi_4^B/\chi_2^B$. Sufficiently far from the critical point, this quantity turns out to be a size-independent quantity in the scaling regime. Below this regime, when the system size is sufficiently small, the emerging dip-peak structure shifts to higher chemical potentials, i.e. lower collision energies, due to finite-size effects. We note that because of the monotonic dependence of the susceptibilities, R_{42} does not exhibit an extremum along the phase boundary at finite L. Its value at the phase transition point decreases monotonically as μ increases, and scales as $L^{9/2}$ and L^6 at the second- and first-order transitions, respectively. This also means that the structure of R_{42} is very similar along the entire phase boundary. Therefore, at finite sizes, the dip-peak structure can be associated with merely the deviation of the freeze-out line from the phase boundary. Therefore, in this case, the non-monotonic behavior does not necessarily indicate the proximity of a critical endpoint.

Although our schematic framework is capable only of qualitative analyses, it provides the possibility of discussing other physical quantities at finite volume. For instance, it can be used to study not only a Lee-Yang edge singularity, but also Lee-Yang zeros in the vicinity of the critical point [56, 57], and the interplay of different special points in the space of complex parameters.

It would also be interesting to directly compare the finite-size effects near a critical point with available lattice calculations [51, 56, 58].

Finally, while our approach is built on the grand canonical picture, a canonical ensemble is expected to be more realistic for very small systems [59, 60]. The canonical effects and their relation to our result will be addressed in our future studies.

ACKNOWLEDGMENTS

We thank Zsolt Szép and Attila Pásztor for insightful discussions. The work is partially supported by the Polish National Science Centre (NCN) under OPUS Grant No. 2022/45/B/ST2/01527. G. K. acknowledges support from the Hungarian National Research, Development and Innovation Fund under Project number K 138277. K.R. acknowledges the support of the Polish Ministry of Science and Higher Education. C.S. acknowledges the support of the World Premier International Research Center Initiative (WPI) under MEXT, Japan.

Appendix A: Thermodynamic quantities at finite size

For completeness, here we define the physical quantities in the presented framework derived from the free energy in Eq. (2), which also serves as a cumulant generating function. We start with the chiral quantities that can be obtained by derivatives with respect to h. Accordingly, the chiral condensate reads (we keep the $S = \beta V \mathcal{U}_{\text{eff}}$ in the exponents to ease the notation)

$$\langle \phi \rangle = -\frac{1}{V} \frac{\delta \Phi}{\delta h} = \frac{1}{\mathcal{Z}} \int \mathcal{D}\phi \ \phi \ e^{-S} \,,$$
 (A1)

while the chiral susceptibilities (we use $\chi_1 \equiv \langle \phi \rangle$, $\chi_2 = \chi$ in the main text) are

$$\chi_{2} = \frac{\delta\langle\phi\rangle}{\delta h} = \frac{1}{\beta V} \left(\frac{1}{\mathcal{Z}} \frac{\delta^{2} \mathcal{Z}}{\delta h^{2}} - \left(\frac{1}{\mathcal{Z}} \frac{\delta \mathcal{Z}}{\delta h} \right)^{2} \right)
= \beta V \left(\langle\phi^{2}\rangle - \langle\phi\rangle^{2} \right) ,
\chi_{3} = (\beta V)^{2} \left(\langle\phi^{3}\rangle - 3\langle\phi\rangle^{2}\langle\phi\rangle + 2\langle\phi\rangle^{3} \right)
\chi_{4} = (\beta V)^{3} \left(\langle\phi^{4}\rangle - 4\langle\phi^{3}\rangle\langle\phi\rangle
+ 12\langle\phi^{2}\rangle\langle\phi\rangle^{2} - 3\langle\phi^{2}\rangle^{2} - 6\langle\phi\rangle^{4} \right) .$$
(A2)

where $\langle \phi^k \rangle$ is the $k^{\rm th}$ raw moment. These susceptibilities are directly related to the cumulants, while their relation to the central moment is as usual.

The thermodynamic quantities can be defined analogously as in the grand canonical ensemble with

$$\Phi = \langle E \rangle - TS - \mu \langle N \rangle \tag{A3}$$

and

$$d\Phi = -SdT - PdV - Nd\mu \tag{A4}$$

Accordingly, the expectation value of the particle number (quark number, in our case 1/3 of the baryon number) reads

$$\langle N \rangle = -\frac{\partial \Phi}{\partial \mu} = \frac{V}{Z} \int \mathcal{D}\phi \, \dot{\mathcal{U}}_{\text{eff}} \, e^{-S}$$
 (A5)

where $\dot{f} \equiv \partial f/\partial \mu$. The cumulants of the particle number can be obtained by further derivatives as

$$\kappa_{k+1} = \frac{\partial^k \langle N \rangle}{\partial \mu^k} \tag{A6}$$

for nonnegative k (for k=0, $\kappa_1=\langle N\rangle$). To remove the extensive volume dependence and allow direct comparison to infinite volume results, in the calculations we use the particle number density $n=\langle N\rangle/V$ and the generalized susceptibilities $\chi_k^B/3=\chi_k^q=\kappa_k/(VT^3)$. For the fluctuations, one can also use the cumulant densities κ_k/V , however, χ_k^B is more widely used in the literature.

In Eq. (A5), one might identify the particle number for a given field configuration to be $N(\phi) = -V \dot{\mathcal{U}}_{eff}$. Interestingly, the second raw moment of the particle number (using \mathcal{Z} to define the moment generating function as $M(\lambda) = \mathcal{Z}(\mu + \lambda/\beta)/\mathcal{Z}(\mu)$) reads

$$\langle N^2 \rangle = \frac{1}{\mathcal{Z}} \int \mathcal{D}\phi (V^2 \dot{\mathcal{U}}_{\text{eff}}^2 - TV \, \ddot{\mathcal{U}}_{\text{eff}}) e^{-S}$$

$$= \langle N^2 \rangle + T \langle \dot{N} \rangle \,. \tag{A7}$$

Here, the second term corresponds to the chemical potential dependence of the particle number corresponding to a

given field configuration. This emerges since we calculate expectation values as an average over the possible field configurations (now trivially, the value of ϕ) instead of the microstates with given N. Calculating the second raw moment density $\langle N^2 \rangle / V^2$, one can see that

$$\langle N^2 \rangle / V^2 = \langle \dot{\mathcal{U}}_{\text{eff}}^2 \rangle + T / V \langle - \ddot{\mathcal{U}}_{\text{eff}} \rangle,$$
 (A8)

i.e., the extra term is suppressed for large volumes and small temperatures, as expected.

We emphasize that the baryon number fluctuations come as the derivative of Φ , and not as a derivative of the pressure, which is defined as the derivative of the free energy with respect to volume

$$P \equiv -\frac{\partial \Phi}{\partial V} = \frac{1}{\mathcal{Z}} \int \mathcal{D}\phi \, \mathcal{U}_{\text{eff}} \, e^{-S} \tag{A9}$$

and hence, $P \neq -\Phi/V$. Moreover, the derivations with respect to different parameters, V, μ , β , and h are not interchangeable with each other and with the averaging $\langle \cdot \rangle$. (Generally, it is also clear that the quantities derived from the grand free energy depend on all those parameters, unless a coincidental cancellation happens.) For convenience, and to distinguish from the $P(\phi)$ probability distribution Eq. (3), we denote the pressure with lower case p in the main text.

For completeness, we also define the entropy

$$S = -\frac{\partial \Phi}{\partial T} = -\frac{\Phi}{T} + \frac{1}{T} \frac{\partial (-\ln Z)}{\partial \beta}$$
 (A10)

and the energy

$$\langle E \rangle = \frac{\partial(-\ln \mathcal{Z})}{\partial \beta} - \frac{\mu}{\beta} \frac{\partial(-\ln \mathcal{Z})}{\partial \mu} = \Phi + TS + \mu \langle N \rangle$$
(A11)

as well. The corresponding entropy and energy density can be obtained as s = S/V and $\epsilon = \langle E \rangle/V$, respectively.

- [1] M. A. Stephanov, Prog. Theor. Phys. Suppl. 153, 139 (2004), arXiv:hep-ph/0402115.
- [2] K. Fukushima and C. Sasaki, Prog. Part. Nucl. Phys. 72, 99 (2013), arXiv:1301.6377 [hep-ph].
- [3] X. Luo and N. Xu, Nucl. Sci. Tech. **28**, 112 (2017), arXiv:1701.02105 [nucl-ex].
- [4] A. Bzdak, S. Esumi, V. Koch, J. Liao, M. Stephanov, and N. Xu, Phys. Rept. 853, 1 (2020), arXiv:1906.00936 [nucl-th].
- [5] K. Binder, Z. Phys. B 43, 119 (1981).
- [6] K. Binder and D. P. Landau, Phys. Rev. B 30, 1477 (1984).
- [7] K. Binder, M. Nauenberg, V. Privman, and A. P. Young, Phys. Rev. B 31, 1498 (1985).
- [8] K. Binder, Lect. Notes Phys. 409, 59 (1992).
- [9] V. Privman and M. Fisher, J Stat Phys **33**, 385– (1983).

- [10] J. Zinn-Justin, Quantum field theory and critical phenomena, International Series of Monographs on Physics, Vol. 77 (Oxford University Press, 2021).
- [11] J. Langelage and O. Philipsen, JHEP 01, 089 (2010), arXiv:0911.2577 [hep-lat].
- [12] V. Vovchenko, J. Steinheimer, O. Philipsen, A. Pasztor, Z. Fodor, S. D. Katz, and H. Stoecker, Nucl. Phys. A 982, 859 (2019), arXiv:1807.06472 [hep-lat].
- [13] S. Borsanyi, G. Endrodi, Z. Fodor, S. D. Katz, and K. K. Szabo, JHEP 07, 056 (2012), arXiv:1204.6184 [hep-lat].
- [14] F. Karsch and E. Laermann, arXiv:hep-lat/0305025.
- [15] A. Bazavov et al., Phys. Rev. D 100, 094510 (2019), arXiv:1908.09552 [hep-lat].
- [16] P. de Forcrand, S. Kim, and T. Takaishi, Nucl. Phys. B Proc. Suppl. 119, 541 (2003), arXiv:hep-lat/0209126.
- [17] G. Parisi, Phys. Lett. B 131, 393 (1983).

- [18] J. R. Klauder, J. Phys. A 16, L317 (1983).
- [19] R. Kara, S. Borsányi, Z. Fodor, J. N. Guenther, P. Parotto, A. Pásztor, and C. H. Wong, EPJ Web Conf. 296, 14004 (2024), arXiv:2401.01169 [hep-lat].
- [20] S. Borsányi, Z. Fodor, J. N. Guenther, R. Kara, P. Parotto, A. Pásztor, L. Pirelli, and C. H. Wong, Phys. Rev. D 111, 014506 (2025).
- [21] G. Colangelo, S. Durr, and R. Sommer, Nucl. Phys. B Proc. Suppl. 119, 254 (2003), arXiv:hep-lat/0209110.
- [22] G. Colangelo and S. Durr, Eur. Phys. J. C 33, 543 (2004), arXiv:hep-lat/0311023.
- [23] G. Colangelo, S. Durr, and C. Haefeli, Nucl. Phys. B 721, 136 (2005), arXiv:hep-lat/0503014.
- [24] J. Gasser and H. Leutwyler, Phys. Lett. B 184, 83 (1987).
- [25] J. Gasser and H. Leutwyler, Phys. Lett. B 188, 477 (1987).
- [26] J. Bijnens and K. Ghorbani, Phys. Lett. B 636, 51 (2006), arXiv:hep-lat/0602019.
- [27] P. H. Damgaard and H. Fukaya, JHEP 01, 052 (2009), arXiv:0812.2797 [hep-lat].
- [28] P. Adhikari and B. C. Tiburzi, Phys. Rev. D 107, 094504 (2023), arXiv:2302.09179 [hep-lat].
- [29] L. F. Palhares, E. S. Fraga, and T. Kodama, J. Phys. G 38, 085101 (2011), arXiv:0904.4830 [nucl-th].
- [30] L. M. Abreu, E. S. Nery, and A. P. C. Malbouisson, Phys. Rev. D 91, 087701 (2015).
- [31] L. M. Abreu and E. S. Nery, Phys. Rev. C **96**, 055204 (2017), arXiv:1711.07934 [nucl-th].
- [32] J. Luecker, C. S. Fischer, and R. Williams, Phys. Rev. D 81, 094005 (2010), arXiv:0912.3686 [hep-ph].
- [33] R.-A. Tripolt, J. Braun, B. Klein, and B.-J. Schaefer, Phys. Rev. D 90, 054012 (2014), arXiv:1308.0164 [hepph].
- [34] J. Bernhardt, C. S. Fischer, P. Isserstedt, and B.-J. Schaefer, Phys. Rev. D 104, 074035 (2021), arXiv:2107.05504 [hep-ph].
- [35] N. Magdy, M. Csanád, and R. A. Lacey, J. Phys. G 44, 025101 (2017), arXiv:1510.04380 [nucl-th].
- [36] G. Kovács, P. Kovács, P. M. Lo, K. Redlich, and G. Wolf, in 7th FAIR next generation scientists workshop 2022 (2023) arXiv:2302.12925 [hep-ph].
- [37] G. Kovács, P. Kovács, P. M. Lo, K. Redlich, and G. Wolf, Phys. Rev. D 108, 076010 (2023), arXiv:2307.10301 [hep-ph].
- [38] S. Collaboration (STAR Collaboration), Phys. Rev. Lett. 126, 092301 (2021).
- [39] M. Abdallah et al. (STAR), Phys. Rev. C 107, 024908

- (2023), arXiv:2209.11940 [nucl-ex].
- [40] J. Adamczewski-Musch et al. (HADES), Phys. Rev. C 102, 024914 (2020), arXiv:2002.08701 [nucl-ex].
- [41] M. Kitazawa and M. Asakawa, Phys. Rev. C 86, 024904 (2012), [Erratum: Phys.Rev.C 86, 069902 (2012)], arXiv:1205.3292 [nucl-th].
- [42] A. Sorensen and P. Sorensen, (2024), arXiv:2405.10278 [nucl-th].
- [43] M. Laine and A. Vuorinen, Basics of Thermal Field Theory, Vol. 925 (Springer, 2016) arXiv:1701.01554 [hep-ph].
- [44] K. Binder, Z. Phys. B **61**, 13 (1985).
- [45] P. Parotto, M. Bluhm, D. Mroczek, M. Nahrgang, J. Noronha-Hostler, K. Rajagopal, C. Ratti, T. Schäfer, and M. Stephanov, Phys. Rev. C 101, 034901 (2020), arXiv:1805.05249 [hep-ph].
- [46] P. Kovacs and Z. Szep, Phys. Rev. D 75, 025015 (2007), arXiv:hep-ph/0611208.
- [47] Q. Wang, Y. Xiq, and H. Zong, Mod. Phys. Lett. A 33, 1850232 (2018), arXiv:1806.05315 [hep-ph].
- [48] X. An, F. Giglio, and G. Landolfi (2025) arXiv:2503.15719 [cond-mat.stat-mech].
- [49] G. Almasi, R. Pisarski, and V. Skokov, Phys. Rev. D 95, 056015 (2017), arXiv:1612.04416 [hep-ph].
- [50] M. Haensch, F. Rennecke, and L. von Smekal, Phys. Rev. D 110, 036018 (2024), arXiv:2308.16244 [hep-ph].
- [51] R. Ashikawa, M. Kitazawa, S. Ejiri, and K. Kanaya, Phys. Rev. D 110, 074508 (2024), arXiv:2407.09156 [hep-lat].
- [52] J. Bernhardt and C. S. Fischer, Phys. Rev. D 108, 114018 (2023), arXiv:2309.06737 [hep-ph].
- [53] A. Andronic, P. Braun-Munzinger, K. Redlich, and J. Stachel, Nature 561, 321 (2018), arXiv:1710.09425 [nucl-th].
- [54] J. Cleymans, H. Oeschler, K. Redlich, and S. Wheaton, J. Phys. G 32, S165 (2006), arXiv:hep-ph/0607164.
- [55] P. Kovács, Z. Szép, and G. Wolf, Phys. Rev. D 93, 114014 (2016), arXiv:1601.05291 [hep-ph].
- [56] T. Wada, M. Kitazawa, and K. Kanaya, Phys. Rev. Lett. 134, 162302 (2025), arXiv:2410.19345 [hep-lat].
- [57] A. Adam, S. Borsányi, Z. Fodor, J. N. Guenther, P. Kumar, P. Parotto, A. Pásztor, and C. H. Wong, (2025), arXiv:2507.13254 [hep-lat].
- [58] A. Kiyohara, M. Kitazawa, S. Ejiri, and K. Kanaya, Phys. Rev. D 104, 114509 (2021), arXiv:2108.00118 [hep-lat].
- [59] R. Hagedorn and K. Redlich, Z. Phys. C 27, 541 (1985).
- [60] J. Cleymans, H. Oeschler, and K. Redlich, Phys. Rev. C 59, 1663 (1999), arXiv:nucl-th/9809027.